Nonlinear dynamics of Aharonov-Bohm cages

Phys. Rev. A 100, 043829 – Published 22 October 2019

Nonlinear dynamics of Aharonov-Bohm cages

Marco Di Liberto,[1,*] Sebabrata Mukherjee,[2,3] and Nathan Goldman[1]

[1]*Center for Nonlinear Phenomena and Complex Systems, Université Libre de Bruxelles, CP 231, Campus Plaine, B-1050 Brussels, Belgium*

[2]*Scottish Universities Physics Alliance (SUPA), Institute of Photonics and Quantum Sciences, School of Engineering and Physical Sciences, Heriot-Watt University, Edinburgh EH14 4AS, United Kingdom*

[3]*Department of Physics, The Pennsylvania State University, University Park, Pennsylvania 16802, USA*

(Received 18 October 2018; revised manuscript received 26 February 2019; published 22 October 2019)

The interplay of π-flux and lattice geometry can yield full localization of quantum dynamics in lattice systems, a striking interference phenomenon known as Aharonov-Bohm caging. At the single-particle level, this full-localization effect is attributed to the collapse of Bloch bands into a set of perfectly flat (dispersionless) bands. While interparticle interactions generally break the cages, not much is known regarding the fate of Aharonov-Bohm caging in the presence of classical nonlinearities, as captured by a discrete nonlinear Schrödinger equation. This scenario is relevant to recent experimental realizations of photonic Aharonov-Bohm cages, using classical light propagating in arrays of coupled waveguides. In this article, we demonstrate that caging always occurs in this nonlinear setting, as long as the nonlinearities remain local. As a central result, we identify special caged solutions that are accompanied by a breathing dynamics of the field intensity that we describe in terms of an effective two-mode model reminiscent of a bosonic Josephson junction. Also, motivated by a formal similarity with the Gross-Pitaevskii equation describing interacting bosons, we explore the quantum regime of Aharonov-Bohm caging using small ensembles of interacting particles, and reveal quasicaged collapse-revival dynamics. The results stemming from this work open an interesting route towards the characterization of nonlinear dynamics in interacting flat-band systems.

DOI: 10.1103/PhysRevA.100.043829

I. INTRODUCTION

The realization of synthetic gauge fields in quantum-engineered matter [1–3] and photonics [4,5] has revolutionized the realm of quantum simulation, by offering the possibility of studying exotic states of matter in a well-controlled environment. In lattice systems, this has led to the exploration of topological phenomena reminiscent of the quantum Hall effects and topological insulators [5–7] and to the study of frustrated magnetism [8–10].

While arbitrary synthetic magnetic fluxes can be realized in artificial lattices [11], such as optical lattices for ultracold gases or photonics lattices for light, combining these artificial fields with strong interparticle interactions still remains a fundamental challenge. An appealing strategy by which interaction effects can be enhanced in lattice systems consists in designing models that exhibit flat (dispersionless) Bloch bands. In these situations, interactions indeed set the dominant energy scale, hence potentially leading to intriguing strongly correlated phenomena [12–14], examples of which include the celebrated fractional quantum Hall effect [15,16] and the recently discovered high-T_c superconductivity in twisted bilayer graphene [17,18]. This highly motivates the implementation of a wide range of flat-band models in artificial lattice systems [19–22].

Interestingly, specific lattice models exhibit a striking interference phenomenon, called Aharonov-Bohm (AB) caging, by which the single-particle spectrum collapses into a set of perfectly flat (dispersionless) Bloch bands [23]. This remarkable effect can be found in the one-dimensional rhombic lattice [24] or in the two-dimensional dice lattice [25,26], in the presence of a magnetic π-flux (i.e., half a flux quantum) per plaquette [23], and it can be attributed to destructive interferences that fully localize any initially prepared wave function. AB cages were first observed in networks of conducting wires [27,28] and were recently realized in photonic lattices [29,30].

The impact of interactions on AB cages has been investigated in different regimes. At the two-body level, the characteristic full-localization property of AB cages was shown to be substantially altered by interactions, which couple distinct single-particle states localized at adjacent unit cells, and hence introduce a mechanism by which the two-particle wave function can spread over the entire lattice [31,32]. At the many-body level, the new channels offered by the interactions are responsible for the appearance of supersolidity at low filling [33] or pair condensation at commensurate filling [34,35]; see also Refs. [36–38]. However, not much is known regarding the fate of AB cages in the presence of classical nonlinearities, as captured by a nonlinear Schrödinger equation. This scenario is particularly relevant to classical photonic systems, e.g., arrays of coupled optical waveguides or exciton-polariton pillars [39], where the nonlinearity of the medium becomes significant at sufficiently high field intensity. Characterizing the robustness of AB caging in the presence of nonlinearities is particularly motivated by their recent realizations in photonics [29,30], where the propagation of intense light waves

*mar.diliberto@gmail.com

inside coupled-waveguide arrays can be accurately described by a discrete nonlinear Schrödinger equation [40–42]. We point out that quantum corrections to this classical description were discussed in Ref. [43], and we note that such effects could be potentially enhanced in the presence of flat bands.

In this article, we elucidate the fate of AB caging in the presence of local nonlinearities, and we characterize the resulting nonlinear dynamics that could be observed in photonic realizations [29]. We demonstrate the generic survival of AB caging in this setting and focus our study on specific solutions so as to highlight a characteristic breathing dynamics of the field intensity, which we describe using a simple effective two-mode model analogous to a bosonic Josephson junction. This analogy offers an intriguing link with the physics of weakly interacting Bose-Einstein condensates in tilted double wells [44]. Besides, motivated by the formal similarity between the nonlinear Schrödinger equation for the propagation of classical-light fields and the Gross-Pitaevskii equation describing weakly interacting bosons [45], we explore the interplay of caging and interactions deep in the quantum regime, by studying the dynamics of a small ensemble of interacting bosons. These exact-diagonalization studies indicate that quasicaged dynamics could be observed in interacting quantum systems, such as superconducting circuits [46] and ultracold atoms in optical lattices [47].

II. MODEL

We consider the dynamics of a classical field defined on a one-dimensional rhombic (diamond) chain with nonvanishing flux ϕ per plaquette and onsite nonlinearity ("interaction") U, as described by the nonlinear Schrödinger equations [29,39]

$$
\begin{aligned}
i\,\partial_t a_n &= -J(b_{n-1} + c_{n-1} + e^{i\phi} b_n + c_n) + U|a_n|^2 a_n, \\
i\,\partial_t b_n &= -J(e^{-i\phi} a_{n-1} + a_n) + U|b_n|^2 b_n, \\
i\,\partial_t c_n &= -J(a_{n-1} + a_n) + U|c_n|^2 c_n. \qquad (1)
\end{aligned}
$$

The quantities $a_n(t)$, $b_n(t)$, and $c_n(t)$ are the field amplitudes for the sites A_n, B_n, and C_n in the nth unit cell; see Fig. 1(a) for a definition of the sites indices. The parameter J denotes the hopping amplitude between neighboring sites. For convenience, a gauge choice is made in Eq. (1) such that the flux within each plaquette ϕ enters the model through a single Peierls phase factor [48] in each unit cell.

For a flux $\phi = \pi$ and negligible nonlinearity ($U = 0$), the system displays three flat bands at energies $\epsilon_\pm = \pm 2J$ and $\epsilon_0 = 0$, a regime known as Aharonov-Bohm caging: the spectrum displays only fully localized eigenstates [23]. The corresponding eigenstates can be written as $|v_\pm\rangle = |B_{n-1}\rangle + |C_{n-1}\rangle \mp 2|A_n\rangle - |B_n\rangle + |C_n\rangle$ and $|v_0\rangle = |B_{n-1}\rangle + |C_{n-1}\rangle + |B_n\rangle - |C_n\rangle$, respectively. When $\phi \neq \pi$ the zero-energy flat band survives, but the upper and lower bands become dispersive.

A. Caged solutions in the presence of nonlinearities

We henceforth focus on the caging limit $\phi = \pi$. The full localization of the spectrum is expected to break in the presence of interactions, since the latter couple distinct neighboring localized states, thus introducing a mechanism for the spreading of the wave function across the lattice; see Ref. [31] for the two-body case, and Ref. [35] for the many-body case and a discussion of the interaction terms arising among flat-band states. In contrast, as it can be proven from Eq. (1), caging still occurs in the presence of classical nonlinearities, and the corresponding dynamics is robust with respect to delocalization for any arbitrary initial state. A pivotal role in this mechanism is played by the hub sites A_n, which can block the spreading over time even in the presence of nonlinearities. The resulting dynamics thus remains confined (caged) between two A sites. Locality is a crucial ingredient in this case, since long-range nonlinear terms would instead break the cages. We have validated the previous statements by using random initial configurations: while caged dynamics is always observed in the presence of local or short-ranged (nearest-neighbor) nonlinearities, it is already substantially deteriorated in the case of (see Appendix).

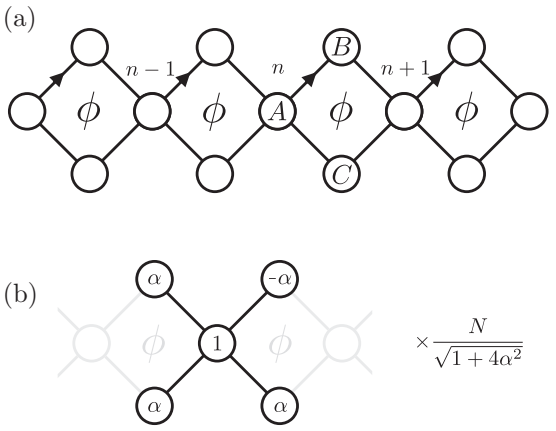

FIG. 1. (a) Rhombic lattice with flux ϕ per plaquette. The gauge choice for the Peierls phase factors in Eqs. (1) is represented by arrows (see intracell A-B bonds). (b) Configuration used as the input for nonlinear caging dynamics; here $0 \leqslant \alpha \leqslant 1$. In the noninteracting limit, this configuration with $\alpha = \pm 1/2$ corresponds to states in the upper and lower bands, respectively. The normalization constant, which depends on the total number of particles N, is shown.

For the sake of simplicity, we restrict ourselves to caged solutions that are characterized by vanishing amplitudes at the lattice sites A_{n-1} and A_{n+1} at all times, thus leaving the dynamics confined in the intermediate five sites; see Fig. 1(b). Setting $a_{n-1}(t) = a_{n+1}(t) = 0$ together with $\dot{a}_{n-1}(t) = \dot{a}_{n+1}(t) = 0$ yields the conditions $b_{n-1}(t) = c_{n-1}(t)$ and $b_n(t) = -c_n(t)$. We decompose the three independent complex numbers $b_{n-1}(t)$, $a_n(t)$, and $b_n(t)$ into amplitude and phase, and we consider the case of a symmetric time evolution $|b_{n-1}(t)| = |b_n(t)|$. After some algebra, one finds that this ansatz for the dynamics fixes a condition for the phases, namely, $\arg[b_n(t)/b_{n-1}(t)] = \pi$ unless $|a_n(t)| = 0$. We therefore conclude that states of the form shown in Fig. 1(b) are caged solutions to the nonlinear equations of motion (1). We point out that this specific field configuration actually shares the same phase profile as that of the lowest-energy eigenstates $|v_-\rangle$ associated with the single-particle spectrum.

Consequently, we are left with only two independent quantities, which we parametrize as

$$a_n(t) \equiv \sqrt{\frac{N-n(t)}{2}}\, e^{i\theta(t)},$$
$$b_{n-1}(t) \equiv \sqrt{\frac{N+n(t)}{8}}\, e^{i\varphi(t)}, \tag{2}$$

where we have defined the conserved total number of particles in the cage $N = |a_n|^2 + 4|b_{n-1}|^2$. The relevant degrees of freedom are the fractional particle imbalance $z(t) \equiv n(t)/N$, with $-1 \leqslant z \leqslant 1$, and the phase difference $\xi(t) \equiv \theta(t) - \varphi(t)$, which satisfy the following coupled nonlinear equations,

$$\dot{z}(t) = -4J\sqrt{1-z(t)^2}\,\sin\xi(t),$$
$$\dot{\xi}(t) = 4J\frac{z(t)}{\sqrt{1-z(t)^2}}\cos\xi(t) + \frac{5}{8}gz(t) - \frac{3}{8}g, \tag{3}$$

where we have defined the nonlinear coupling $g \equiv NU$.

Interestingly, the coupled equations (3) can be obtained from the classical Hamiltonian

$$\mathcal{H} = -4J\sqrt{1-z^2}\cos\xi + \frac{5}{16}gz^2 - \frac{3}{8}gz, \tag{4}$$

by considering ξ as a generalized coordinate and z as its canonically conjugate momentum. In this respect, Eqs. (3) and (4) describe the dynamics of a nonrigid pendulum, and $\mathcal{H}$ describes the conserved energy of the system. This shows how restricting the dynamics to the solutions in Eq. (2), whose equations of motion correspond to Eqs. (3), allows one to map the initial problem onto a two-mode model for an amplitude degree of freedom and a phase degree of freedom. This mapping offers an intriguing reinterpretation of the nonlinear AB-caging dynamics in terms of that associated with a weakly interacting Bose condensate in a tilted double well [49,50] or in two hyperfine states [51]. In other words, this nontrivial dynamics corresponds to that of a generalized bosonic Josephson junction [44,52], which displays, for instance, macroscopic self-trapping for high-energetic excitations [53] and "twist-and-turn" spin squeezing [51].

Moreover, the ground state of $\mathcal{H}$, occurring for $\xi = 0$ and for values of z_0 that depend on the ratio g/J, corresponds to a stationary discrete soliton solution that can be continuously connected to the single particle eigenstates when $g/J \to 0$. These solutions typically occur in flat-band systems, occupy few sites, and have no exponential tail [42,54–57].

B. Time evolution of nonlinear caged states

We now focus on the time evolution in the presence of π-flux, and we reveal that nonlinear caging is characterized by a breathing dynamics of the field intensity inside the cage.

Based on the results presented in the previous paragraph, we consider an initial state at $t = 0$ of the form $b_{n-1}(0) = c_{n-1}(0) = -b_n(0) = c_n(0)$ and $a_n(0) \neq 0$, and we define the parameter $\alpha = b_{n-1}(0)/a_n(0)$. Furthermore, we fix the initial phase difference to $\xi(0) = 0$ [see Fig. 1(b)], which amounts to take a real valued $\alpha > 0$. Together with the "interaction" parameter, $g = NU$, these parameters uniquely determine the initial conditions of the problem. For simplicity, we will consider units where $U = J = 1$ in the rest of the discussion, which potentially corresponds to a regime of large nonlinearities.

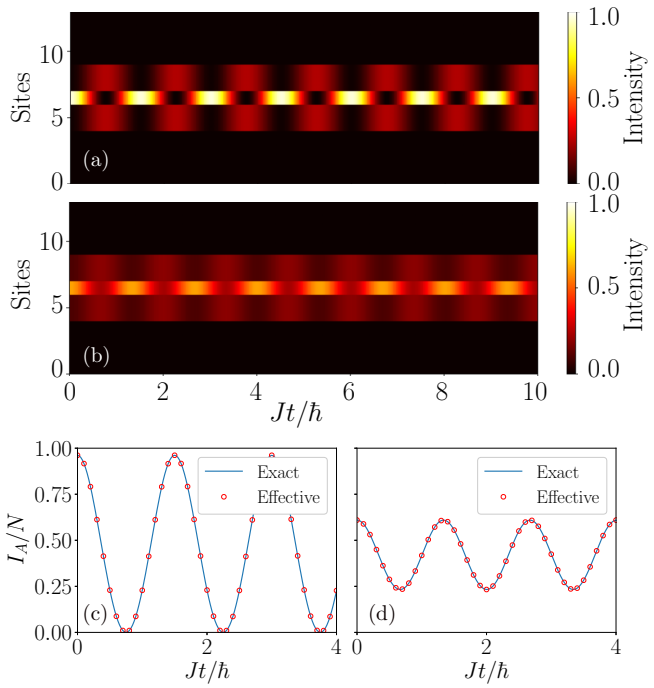

FIG. 2. (a) and (b) Time evolution of the normalized intensity (particle density), $I = |\psi_n|^2/N$, on a diamond chain with π-flux and $L = 13$ sites, for $g = 2.5J$: (a) $\alpha = 0.1$ and (b) $\alpha = 0.4$. Here the density is normalized with respect to the total number of particles N. A breathing motion together with the caging of the total intensity is observed. (c) and (d) Time evolution of the intensity I_A, associated with the central A site in Fig. 1(b), as obtained from the exact nonlinear Schrödinger evolution (line) and from the effective two-mode model (circles). All parameters are the same as in panels (a) and (b).

In Figs. 2(a) and 2(b) we show the resulting periodic dynamics, for a nonlinear regime corresponding to $g = 2.5J$, and for two different initial conditions ($\alpha = 0.1$ and $\alpha = 0.4$). In Figs. 2(c) and 2(d), we demonstrate that the full nonlinear Schrödinger dynamics can be quantitatively described by the two-mode dynamical equations (3). The dynamics that we have presented so far corresponds to the case where one prepares an initial state that is characterized by a nonvanishing displacement $z(0) \neq 0$ with respect to the minimum (ground state) of the classical Hamiltonian $\mathcal{H}$ in Eq. (4); see discussion above on the stationary solutions of the equations of motion and the white dashed line in Fig. 3(a). When $z(0) \approx z_0$, the system is in the regime of small oscillations and one expects purely harmonic dynamics, whereas the dynamics becomes anharmonic when $z(0)$ is sufficiently far from z_0 (as revealed, for instance, by the Fourier spectrum).

We have investigated caging in a large region of parameter space, and we characterize the resulting periodic breathing dynamics by representing its main (smallest) frequency ω in Fig. 3, for both $g > 0$ and $g < 0$. The main frequency of these oscillations displays a nonmonotonic behavior as a function of g, and it is given by $\omega = 4J$ when $g \to 0$, as expected from

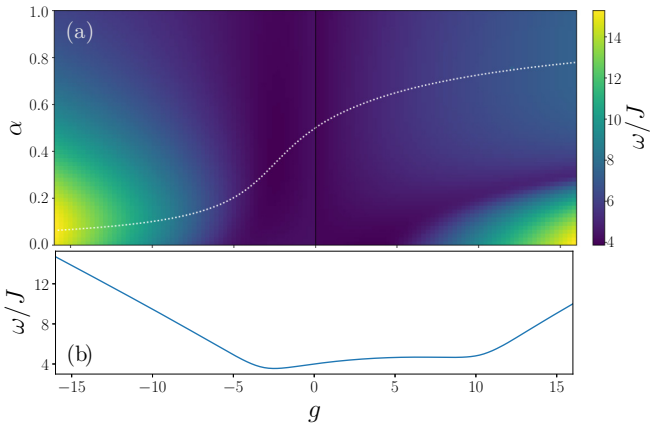

FIG. 3. (a) Main frequency of the breathing dynamics for (attractive) $g < 0$ and (repulsive) $g > 0$ interactions. The white dashed line corresponds to the minimum of the classical Hamiltonian $\mathcal{H}$ in Eq. (4) occurring for $\xi = 0$, namely, a stationary discrete soliton solution of the nonlinear Schrödinger equations. When $g \to 0$, the minimum reaches $\alpha \to 1/2$, which corresponds to the localized states of the single-particle lowest energy band. (b) Cut in panel (a) at $\alpha = 0.2$.

the fact that the initial state overlaps with the upper and lower flat bands of the single-particle spectrum in this limit. We note that the periodicity of the oscillations at small negative g is in agreement with the results of Ref. [58].

III. QUANTUM DYNAMICS

The classical regime explored in the previous section, raises the question whether caged dynamics might also take place in the quantum regime. It is known that quantum processes couple neighboring unit cells through particle collisions and that caging is therefore expected to break down in the quantum regime [31,32,35]. Here we show that despite pairs of particles can freely delocalize, states with larger number of particles per site can have a short-time *quasicaged* dynamics within reasonable timescales before full delocalization takes place.

We have performed exact-diagonalization calculations with $N = 2, 3, 4, 5$ particles in a rhombic chain with $L = 13$ sites [four complete rhombis; see Fig. 4(a)] using a Bose-Hubbard model with onsite interactions described by the Hamiltonian

$$\hat{H} = -J \sum_{\langle i,j \rangle} (e^{i\theta_{ij}} \hat{\psi}_i^\dagger \hat{\psi}_j + \text{H.c.}) + \frac{U}{2} \sum_i \hat{n}_i(\hat{n}_i - 1), \quad (5)$$

where the Peierls phases θ_{ij} are chosen such as to have a π-flux per plaquette and the fields $\hat{\psi}_i$ describe particles on the A, B, C sites (when $i = 3n$, $\hat{\psi}_{3n} \equiv \hat{a}_n$, $\hat{\psi}_{3n+1} \equiv \hat{b}_n$, and $\hat{\psi}_{3n+2} \equiv \hat{c}_n$). In direct analogy with the classical state in Fig. 1(b) with $\alpha = 0$, we have chosen an initial state with all particles in the central A site,

$$|\psi(t = 0)\rangle = \frac{1}{\sqrt{N!}} (\hat{a}_n^\dagger)^N |0\rangle, \quad (6)$$

and explored several values of the onsite interaction U, keeping the product $g = NU$ fixed.

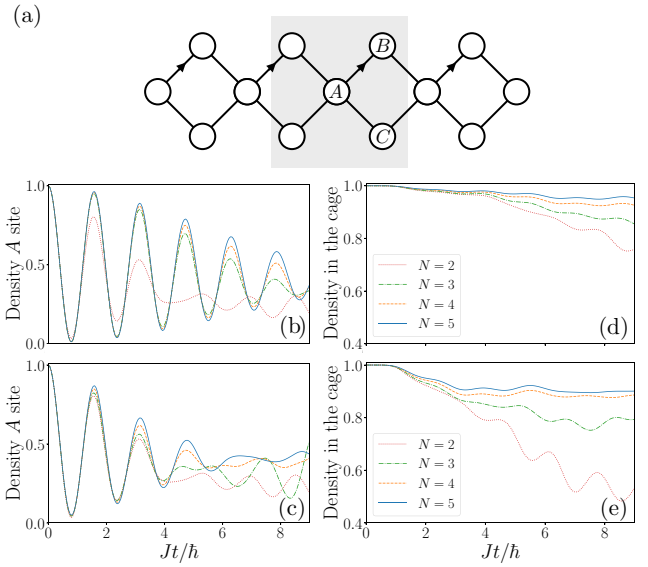

FIG. 4. (a) Lattice with $L = 13$ sites and π-flux used for the exact-diagonalization calculations in the quantum regime. The arrows indicate the gauge choice used here and in the main text. The shadowed region includes the sites forming the smallest cage in the classical limit. (b) and (c) Normalized density time evolution of the central A site for (b) $g = 1.2\,J$ and (c) $g = 2.4\,J$ with $N = 2, 3, 4, 5$ bosons. (d) and (e) Normalized total density inside the cage sites highlighted in panel (a) with the same values of g as in (b) and (c).

In Figs. 4(b) and 4(c), we plot the short timescale evolution of the density in the central A site for different values of N, which shows a clear damped oscillation. In Figs. 4(d) and 4(e), we plot the density within the five cage sites of Fig. 4(a) normalized with respect to the total number of particles N. The number of leaked particles $\Delta N = N - N_c$ (shown in Fig. 5) does not strongly depend on N for $N > 3$ and remains bounded to $\Delta N \leqslant 0.5$, such that most of the particles ($\approx$90%) remain in the cage sites after a time $t \approx 40\hbar/J$ thus entering a "quasicaged" regime.

The suppression of leaked density raises the question whether quantum caged dynamics with well-defined properties already takes place with few particles per site. This is not the case with $N = 2$ already at small $g < J$: after a few damped oscillations the density completely spreads outside the cage. However, when increasing the number of particles one observes a peculiar evolution inside the cage that shows collapse and revival features [see Figs. 6(a) and 6(b)] that are reminiscent of collapse-revival dynamics occurring in

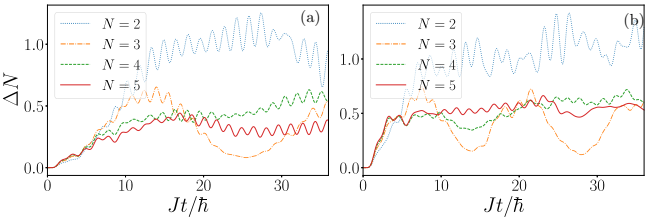

FIG. 5. Leaked number of particles $\Delta N = N - N_c$, where N_c is the total number of particles in the cage at time t. Parameters chosen as in Figs. 4(d) and 4(e) but with a longer timescale.

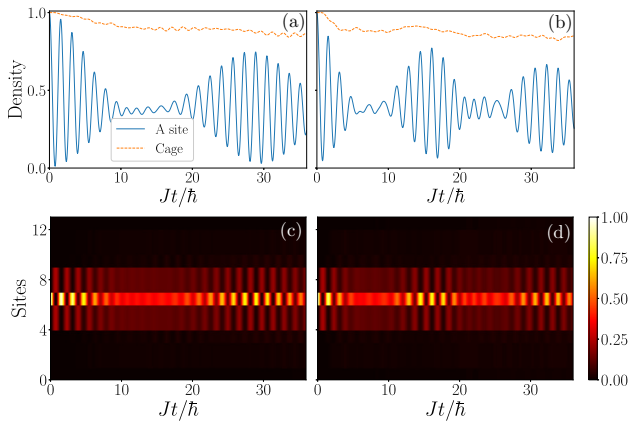

FIG. 6. (a) and (b) Normalized density time evolution for $N = 4$ bosons and (a) $g = 1.2\,J$ and (b) $g = 2.4\,J$ showing collapse and revival features (blue line). The dashed red line tracks the total density inside the cage of Fig. 4(a). (c) and (d) Normalized density time evolution of the full rhombic chain, parameters as in panels (a) and (b).

coherent bosonic systems [45,59–61], whereas the leaked density remains small over several revival periods. In particular, oscillations as in Fig. 6 have been identified in imbalanced double wells in the quantum regime [59]. Moreover, we have also observed in our simulation that the revival period increases with N while keeping g constant, as discussed in Ref. [59]. These facts suggest that the double-well picture presented in Sec. II A in the classical case may be extended to the quantum regime as well. Elucidating the possible crossover from the quantum "quasicaged" to the classical "caged" regimes explored in this work therefore appears as an intriguing perspective.

IV. CONCLUSIONS AND EXPERIMENTAL CONSIDERATIONS

We have shown that AB caging survives in a rhombic lattice with π-flux in the presence of local (classical) nonlinearities independently of the strength of the latter. Similarly to the linear ("single-particle") situation [29], caging exists due to the presence of hub sites A_n [see Fig. 1(a)], which block the spreading of the wave function through phase interferences. Here locality is essential in that long-range (i.e., at least next-nearest-neighbor) nonlinearities are required to break the cages. For onsite nonlinearities, and when the cage includes a single site A, the corresponding breathing motion of the density can be understood in terms of a simple two-mode theory with a period of oscillation that displays a nonmonotonic behavior.

Imperfections (e.g., the presence of disorder [62,63], deviations from the initial conditions or from the π-flux limit) can potentially lead to instabilities in the dynamics, which in turn will alter the interference processes and the resulting time evolution. However, if the instabilities associated with these modes are weak, namely, if the instability manifests itself within a timescale τ such that $\omega\tau > 1$, where ω is the frequency of the expected oscillations, one should still be able to observe the nonlinear dynamics associated with the specific (ideal) initial conditions considered in this work. A linear stability analysis performed on the state represented in Fig. 1(b) would allow one to extract the relevant timescale τ and thus identify the optimal set of parameters for a given experimental setting; see also the discussion of stability in the numerical study reported in Ref. [58].

Ultrafast-laser-fabricated waveguide arrays are a promising platform to observe nonlinear caging dynamics, especially in light of the recent experimental realizations [29,30]. In this platform, the propagation of the electric field is described by a nonlinear Schrödinger equation, where the nonlinear term describes the optical Kerr nonlinearity of the medium [5,39,41] and the waveguide-propagation coordinate plays the role of time. The largest "interaction" strength g that can be achieved in coupled-waveguide arrays depends on the nonlinear refractive index of the medium, on the effective area of the waveguide mode, and on the wavelength and the power of the incident light [40]. In order to provide an accurate estimation of realistic nonlinearities, we have performed a preliminary experimental analysis of these effects in a coupled-waveguide array realized in a borosilicate glass substrate. Our measurements indicate that one can reach values of the order of $|g/J| \approx 10$, thus making the exploration of our results possible in current experiments. Also, we note that the short-time ($t \sim 4\hbar/J$) dynamics is relatively easy to access experimentally, which should allow one to observe the aforementioned breathing motion and to measure the corresponding frequency shift caused by nonlinearities. The possibility of detecting long-time dynamics is strongly constrained by the relatively small propagation distance of the waveguides (≈ 10 cm), a limitation that can nevertheless be overcome through state-recycling techniques [64]. Finally, the presence of losses, which would decrease the total guided optical power during its propagation, must be carefully optimized in any experimental realization.

Cold atoms in optical lattices could offer another versatile platform to observe flat-band phenomena [65,66]. Interactions can be tuned in these settings [47], using Feshbach resonances, and disorder (a source of instability) is typically absent. These systems would allow one to investigate the interplay of AB caging and interparticle interactions, deep in the quantum regime.

Note added. Recently, we became aware of another study dedicated to the impact of nonlinearities in photonic Aharonov-Bohm cages [58].

ACKNOWLEDGMENTS

We thank G. Salerno and R. R. Thomson for helpful discussions. N.G. and M.D. acknowledge support from the ERC Starting Grant TopoCold. S.M. thanks Université Libre de Bruxelles (ULB) and Scottish Universities Physics Alliance (SUPA) for hosting and funding through the Postgraduate, Postdoctoral and Early Career Researcher Short-Term Visits Programme-2018, respectively.

APPENDIX: DYNAMICS OF A RANDOM INITIAL STATE WITH SHORT- AND LONG-RANGE NONLINEARITIES

The discrete nonlinear Schrödinger equations defined on the rhombic chain (see main text) always lead to caged

dynamics; the corresponding cage is specifically made of sites that are bounded by two A_n sites, which therefore play the role of a hub. This fact is a consequence of the locality of nonlinearities ("interactions") and can be immediately understood if one considers the two relevant cases:

(1) If a A_n site has a vanishing amplitude at time t and is one of the boundary sites of the cage, the equations of motion for the sites outside the cage will have no dynamics because they are uncoupled from the cage, thus keeping a zero amplitude over time;

(2) If a A_n site has a nonvanishing amplitude at time t and there is no amplitude for $m < n$ (or $m > n$), the dynamics of the external B_{n-1} and C_{n-1} sites (or B_n and C_n) will be symmetric in amplitude and in-phase (or out-of-phase), as for the state considered in the main text. Therefore, destructive interference will take place on the site A_{n-1} (or A_{n+1}), which becomes one of the hubs of the cage as in point (1).

The cases described above build on the locality of nonlinearities, which preserves the interference process that is behind the caging phenomenon. A simple inspection of the equations shows that even nearest-neighbor nonlinearities do not change these conclusions. Indeed, the peripheral B and C sites discussed above in (2) are nevertheless coupled to the same A_n hub site and the symmetry properties of their equations discussed in (2) is not affected.

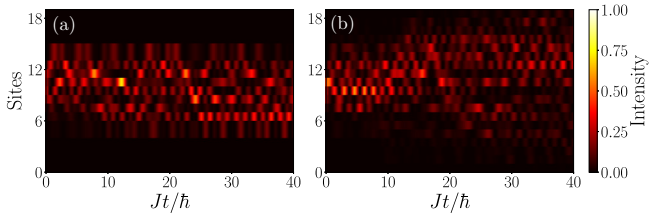

FIG. 7. (a) Classical time evolution of a random configuration with onsite (U) and nearest-neighbor (V_{NN}) nonlinearity showing caged dynamics for $U = V_{NN}$ and $g = 6$. (b) Same as in panel (a) but with next-nearest-neighbor nonlinearity V_{NNN} showing loss of caging and propagation of the field over the entire lattice.

Instead, when next-nearest-neighbor nonlinearities are included, B and C sites in neighboring unit cells are directly coupled. Therefore, a density imbalance or a random phase difference between B and C sites in one unit cell will generate an asymmetric dynamics in the neighboring unit cells. The interference process required for caging cannot take place, thus yielding the field to propagate across the entire lattice.

These conclusions have been tested using a random initial configuration in the case of (1) onsite and nearest-neighbor nonlinearities and (2) onsite and next-nearest-neighbor nonlinearities. In Figs. 7(a) and 7(b), it is shown that caging is indeed preserved for (1) and lost for (2).

[1] N. R. Cooper, Adv. Phys. **57**, 539 (2008).
[2] J. Dalibard, F. Gerbier, G. Juzeliūnas, and P. Öhberg, Rev. Mod. Phys. **83**, 1523 (2011).
[3] N. Goldman, G. Juzeliūnas, P. Öhberg, and I. B. Spielman, Rep. Prog. Phys. **77**, 126401 (2014).
[4] L. Lu, J. D. Joannopoulos, and M. Soljačić, Nat. Photonics **8**, 821 (2014).
[5] T. Ozawa, H. M. Price, A. Amo, N. Goldman, M. Hafezi, L. Lu, M. C. Rechtsman, D. Schuster, J. Simon, O. Zilberberg, and I. Carusotto, Rev. Mod. Phys. **91**, 015006 (2019).
[6] N. Goldman, J. Budich, and P. Zoller, Nat. Phys. **12**, 639 (2016).
[7] N. R. Cooper, J. Dalibard, and I. B. Spielman, Rev. Mod. Phys. **91**, 015005 (2019).
[8] J. Struck, C. Ölschläger, R. Le Targat, P. Soltan-Panahi, A. Eckardt, M. Lewenstein, P. Windpassinger, and K. Sengstock, Science **333**, 996 (2011).
[9] J. Struck, M. Weinberg, C. Ölschläger, P. Windpassinger, J. Simonet, K. Sengstock, R. Höppner, P. Hauke, A. Eckardt, M. Lewenstein *et al.*, Nat. Phys. **9**, 738 (2013).
[10] A. Eckardt, Rev. Mod. Phys. **89**, 011004 (2017).
[11] M. Aidelsburger, S. Nascimbene, and N. Goldman, C. R. Phys. **19**, 394 (2018).
[12] S. D. Huber and E. Altman, Phys. Rev. B **82**, 184502 (2010).
[13] N. Regnault and B. A. Bernevig, Phys. Rev. X **1**, 021014 (2011).
[14] S. Peotta and P. Törmä, Nat. Commun. **6**, 8944 (2015).
[15] D. C. Tsui, H. L. Stormer, and A. C. Gossard, Phys. Rev. Lett. **48**, 1559 (1982).
[16] D. Yoshioka, *The Quantum Hall Effect* (Springer-Verlag Berlin, 2013).
[17] Y. Cao, V. Fatemi, S. Fang, K. Watanabe, T. Taniguchi, E. Kaxiras, and P. Jarillo-Herrero, Nature (London) **556**, 43 (2018).
[18] Y. Cao, V. Fatemi, A. Demir, S. Fang, S. L. Tomarken, J. Y. Luo, J. D. Sanchez-Yamagishi, K. Watanabe, T. Taniguchi, E. Kaxiras *et al.*, Nature (London) **556**, 80 (2018).
[19] S. Mukherjee, A. Spracklen, D. Choudhury, N. Goldman, P. Öhberg, E. Andersson, and R. R. Thomson, Phys. Rev. Lett. **114**, 245504 (2015).
[20] R. A. Vicencio, C. Cantillano, L. Morales-Inostroza, B. Real, C. Mejía-Cortés, S. Weimann, A. Szameit, and M. I. Molina, Phys. Rev. Lett. **114**, 245503 (2015).
[21] S. Taie, H. Ozawa, T. Ichinose, T. Nishio, S. Nakajima, and Y. Takahashi, Sci. Adv. **1** e1500854 (2015).
[22] D. Leykam, A. Andreanov, and S. Flach, Adv. Phys. X **3**, 1473052 (2018).
[23] J. Vidal, R. Mosseri, and B. Douçot, Phys. Rev. Lett. **81**, 5888 (1998).
[24] S. Mukherjee and R. R. Thomson, Opt. Lett. **40**, 5443 (2015).
[25] D. Bercioux, D. F. Urban, H. Grabert, and W. Häusler, Phys. Rev. A **80**, 063603 (2009).
[26] D. Bercioux, N. Goldman, and D. F. Urban, Phys. Rev. A **83**, 023609 (2011).
[27] C. C. Abilio, P. Butaud, T. Fournier, B. Pannetier, J. Vidal, S. Tedesco, and B. Dalzotto, Phys. Rev. Lett. **83**, 5102 (1999).
[28] C. Naud, G. Faini, and D. Mailly, Phys. Rev. Lett. **86**, 5104 (2001).
[29] S. Mukherjee, M. Di Liberto, P. Öhberg, R. R. Thomson, and N. Goldman, Phys. Rev. Lett. **121**, 075502 (2018).

[30] M. Kremer, I. Pedres, E. Meyer, M. Heinrich, O. Zilberberg, and A. Szameit, arXiv:1805.05209.
[31] J. Vidal, B. Douçot, R. Mosseri, and P. Butaud, Phys. Rev. Lett. **85**, 3906 (2000).
[32] C. E. Creffield and G. Platero, Phys. Rev. Lett. **105**, 086804 (2010).
[33] G. Möller and N. R. Cooper, Phys. Rev. Lett. **108**, 045306 (2012).
[34] B. Douçot and J. Vidal, Phys. Rev. Lett. **88**, 227005 (2002).
[35] C. Cartwright, G. De Chiara, and M. Rizzi, Phys. Rev. B **98**, 184508 (2018).
[36] S. Takayoshi, H. Katsura, N. Watanabe, and H. Aoki, Phys. Rev. A **88**, 063613 (2013).
[37] M. Tovmasyan, E. P. L. van Nieuwenburg, and S. D. Huber, Phys. Rev. B **88**, 220510(R) (2013).
[38] M. Tovmasyan, S. Peotta, L. Liang, P. Törmä, and S. D. Huber, Phys. Rev. B **98**, 134513 (2018).
[39] I. Carusotto and C. Ciuti, Rev. Mod. Phys. **85**, 299 (2013).
[40] H. S. Eisenberg, Y. Silberberg, R. Morandotti, A. R. Boyd, and J. S. Aitchison, Phys. Rev. Lett. **81**, 3383 (1998).
[41] A. Szameit and S. Nolte, J. Phys. B **43**, 163001 (2010).
[42] F. Lederer, G. I. Stegeman, D. N. Christodoulides, G. Assanto, M. Segev, and Y. Silberberg, Phys. Rep. **463**, 1 (2008).
[43] P.-E. Larré and I. Carusotto, Phys. Rev. A **92**, 043802 (2015).
[44] R. Gati and M. K. Oberthaler, J. Phys. B **40**, R61 (2007).
[45] L. Pitaevskii and S. Stringari, *Bose-Einstein Condensation and Superfluidity* (Oxford University Press, Oxford, 2016).
[46] R. Ma, B. Saxberg, C. Owens, N. Leung, Y. Lu, J. Simon, and D. I. Schuster, Nature (London) **566**, 51 (2019).
[47] I. Bloch, J. Dalibard, and S. Nascimbène, Nat. Phys. **8**, 267 (2012).
[48] D. R. Hofstadter, Phys. Rev. B **14**, 2239 (1976).
[49] A. Smerzi, S. Fantoni, S. Giovanazzi, and S. R. Shenoy, Phys. Rev. Lett. **79**, 4950 (1997).
[50] S. Raghavan, A. Smerzi, S. Fantoni, and S. R. Shenoy, Phys. Rev. A **59**, 620 (1999).
[51] W. Muessel, H. Strobel, D. Linnemann, T. Zibold, B. Juliá-Díaz, and M. K. Oberthaler, Phys. Rev. A **92**, 023603 (2015).
[52] F. S. Cataliotti, S. Burger, C. Fort, P. Maddaloni, F. Minardi, A. Trombettoni, A. Smerzi, and M. Inguscio, Science **293**, 843 (2001).
[53] M. Albiez, R. Gati, J. Fölling, S. Hunsmann, M. Cristiani, and M. K. Oberthaler, Phys. Rev. Lett. **95**, 010402 (2005).
[54] S. Flach and A. V. Gorbach, Phys. Rep. **467**, 1 (2008).
[55] C. Danieli, A. Maluckov, and S. Flach, Low Temp. Phys. **44**, 678 (2018).
[56] J. L. Marzuola, M. Rechtsman, B. Osting, and M. Bandres, arXiv:1904.10312.
[57] V. Goblot, B. Rauer, F. Vicentini, A. L. Boité, E. Galopin, A. Lemaître, L. L. Gratiet, A. Harouri, I. Sagnes, S. Ravets, C. Ciuti, A. Amo, and J. Bloch, Phys. Rev. Lett. **123**, 113901 (2019).
[58] G. Gligorić, P. P. Beličev, D. Leykam, and A. Maluckov, Phys. Rev. A **99**, 013826 (2019).
[59] G. J. Milburn, J. Corney, E. M. Wright, and D. F. Walls, Phys. Rev. A **55**, 4318 (1997).
[60] M. Greiner, O. Mandel, T. W. Hänsch, and I. Bloch, Nature (London) **419**, 51 (2002).
[61] U. R. Fischer and R. Schützhold, Phys. Rev. A **78**, 061603(R) (2008).
[62] J. Vidal, P. Butaud, B. Douçot, and R. Mosseri, Phys. Rev. B **64**, 155306 (2001).
[63] D. Rivas and M. I. Molina, arXiv:1810.04804.
[64] S. Mukherjee, H. K. Chandrasekharan, P. Öhberg, N. Goldman, and R. R. Thomson, Nat. Commun. **9**, 4209 (2018).
[65] G. Möller and N. R. Cooper, New J. Phys. **20**, 073025 (2018).
[66] G. Pelegrí, A. M. Marques, R. G. Dias, A. J. Daley, V. Ahufinger, and J. Mompart, Phys. Rev. A **99**, 023612 (2019).